MODELS OF UWB PULSES

L. E. Miller, NIST

DRAFT, 2 May 2003

1.0 Examples of UWB Pulses

Perhaps the simplest UWB communication waveform is the monopulse, an example of which is plotted in Figure 1.1. Although it is described as an idealized waveform, it does serve to illustrate the important distinction that must be made between transmitted and received carrierless UWB waveforms, a distinction that is necessary because the effect of the transmitting and receiving antennas on the shape of the waveform as a function of time is very noticeable, unlike the case of longer duration waveforms using carriers. Without getting into the details of the physical generation of UWB waveforms, it is sufficient to note in this regard that the transmitting antenna has the general effect of differentiating the time waveform presented to it. As a consequence the transmitted pulse does not have a DC (direct current) value-the integral of the waveform over its duration must equal zero. The waveform in Fig. 1.1 satisfies this condition and therefore is a plausible model for a UWB waveform; it is ideal in the sense that, in addition to having no DC value, it has even symmetry about the peak value. In general, such symmetry is not achieved in practice, which we will illustrate in what follows with examples of actual waveforms taken from the literature.

A clear example of how the antennas affect the UWB waveform is given in Figure 1.2, in which an impulse-like pulse is differentiated a number of times before being received. Also shown in the figure is the reception of multipath components, a characteristic feature of received UWB signals. Another example of an UWB signal measurement is shown in Figure 1.3, which also indicates the bandwidth occupied by the waveform when the basic pulse is used to generate a communications signal with a baud rate of 850 Kbps. A simplified "doublet" model of a differentiated monopulse is shown in Figure 1.4.

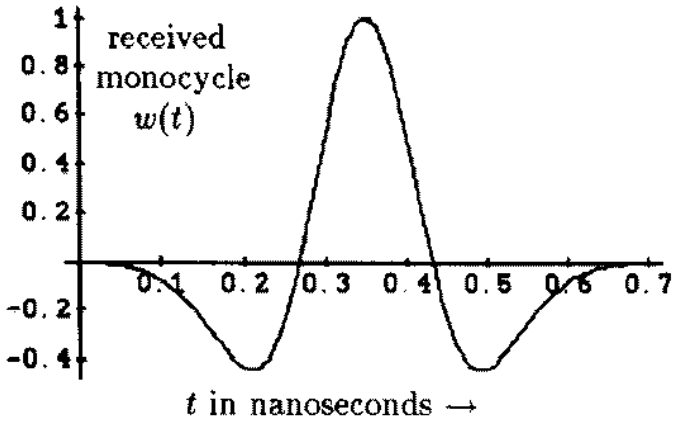

Figure 1.1 Monopulse UWB waveform (from [1]).

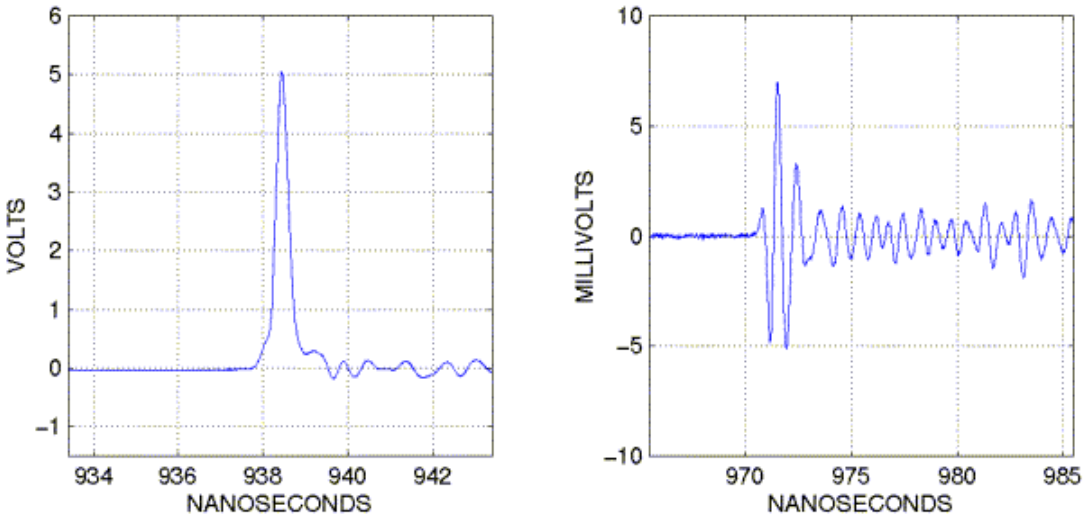

(a) Pulser Output (b) Received Signal

Figure 1.2 Example of the effect of antennas on the UWB pulse shape (from [2])

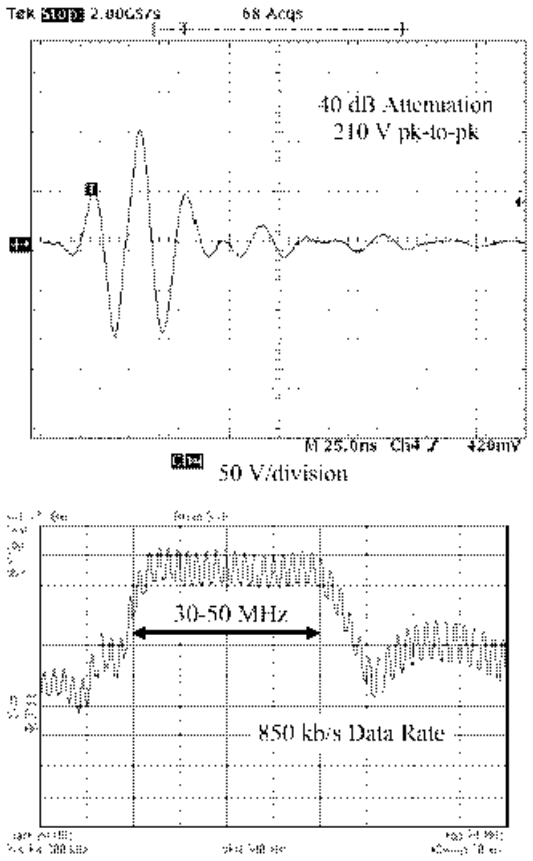

Figure 1.3 Time capture and modulated spectrum of a working UWB communication system (from [3]).

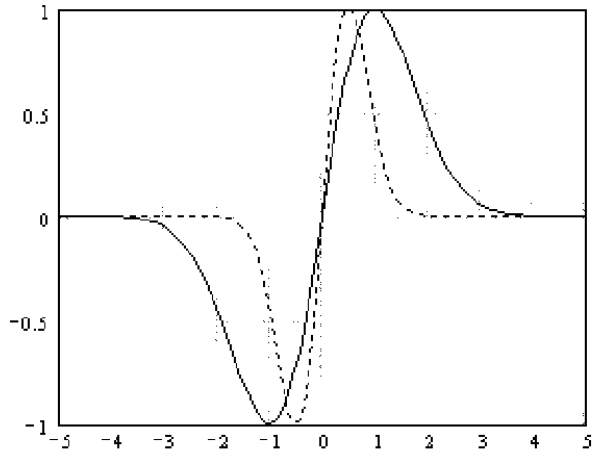

Figure 1.4 Doublet model of an UWB pulse shape (from [4]).

2.0 Mathematical Models of UWB Pulses

For analysis purposes, various idealized models and generalizations of the elemental UWB pulse waveforms have been developed. Here we consider several models: N-cycle sinusoids with various envelopes, a sinusoid with a Gaussian envelope, and a family of pulse shapes based on Hermite polynomials.

2.1 N-cycle Sinusoid Models

2.1.1 N-cycle Sinusoid with Rectangular Envelope

One analytical model is a "polycycle" waveform consisting of N cycles of a sinusoid:

$$s(t) = \begin{cases} \sin(\omega_r t), & 0 \le t < NT \\ 0, & \text{otherwise} \end{cases} \tag{2.1}$$

where $\omega_r = 2\pi/T$. The Fourier transform of this waveform is

$$\begin{aligned} S(\omega) &= \frac{1}{2}\left[\frac{1-\mathrm{e}^{-j(\omega+\omega_r)NT}}{\omega+\omega_r} - \frac{1-\mathrm{e}^{-j(\omega-\omega_r)NT}}{\omega-\omega_r}\right] \\ &= \frac{jNT}{2}\,\mathrm{e}^{-j\omega NT/2}\left[\mathrm{e}^{-jN\pi}\,\mathrm{sinc}\left(\frac{(\omega+\omega_r)NT}{2\pi}\right) - \mathrm{e}^{jN\pi}\,\mathrm{sinc}\left(\frac{(\omega-\omega_r)NT}{2\pi}\right)\right] \end{aligned} \tag{2.2a}$$

where $\mathrm{sinc}(x) = \sin(\pi x)/\pi x$. For N an integer or an integer plus 1/2 (yielding a piecewise continuous waveform),

$$S(\omega) = \left[1-(-1)^{2N}\mathrm{e}^{-j\omega NT}\right]\frac{1/\omega_r}{1-(\omega/\omega_r)^2} \tag{2.2b}$$

This gated waveform and its power spectral density (the squared magnitude of $S(\omega)$) are shown in Figure 2.1 for integer values of N. Note that the spectrum is centered at the frequency of the

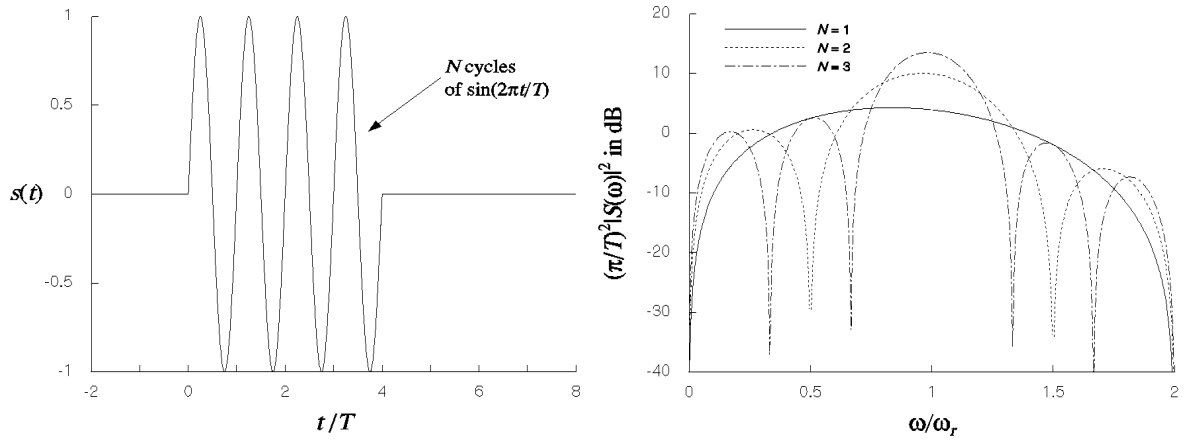

Figure 2.1 Polycycle waveform and power spectral density.

sinusoidal burst and that the bandwidth of the signal is inversely proportional to the number of cycles in the burst, N. The signal transitions from UWB to a conventional signal in terms of bandwidth when N is greater than four [5]. These characteristics give some freedom to position the waveform in the spectrum and could be the basis for the generation of multiple UWB frequency-division multiplex (FDM) channels as in conventional communication systems [6]. The equivalent rectangular (noise) bandwidth of the bandpass signal, denoted B (in Hz), equals that of the envelope (modulation), which in this case is a rectangular function, which has a $\text{sinc}^2(\omega NT/2\pi)$ spectrum. Using formula 3.821.9 of [7], B is found to be

$$2\pi B = \int_{-\infty}^{\infty} d\omega \,\text{sinc}^2\left(\frac{\omega}{2\pi}NT\right) = \frac{2}{NT}\int_{-\infty}^{\infty} dx\,\frac{\sin^2 x}{x^2} = \frac{2\pi}{NT} = \frac{\omega_r}{N} \tag{2.2c}$$

The noise bandwidth is illustrated in Figure 2.2 for $N = 2$, 4, and 6. It is interesting that the 3-dB bandwidth, denoted B_3, is found to be

$$\text{sinc}^2\left(\frac{B_3 NT}{2}\right) = 0.5 \quad \Rightarrow \quad 2\pi B_3 = 0.886\,\frac{2\pi}{NT} = 0.886\,\frac{\omega_r}{N} \tag{2.2d}$$

B_3 is smaller than the noise bandwidth, which in this case equals the 3.9-dB bandwidth.

The autocorrelation function for the polycycle model, plotted in Figure 2.3, is given by

$$\text{R}_s(\tau) = \begin{cases} (NT - |\tau|)\cdot\dfrac{1}{2}\cos(\omega_r\tau) + \dfrac{1}{2\omega_r}\cos(2\pi N)\sin[\omega_r(NT - |\tau|)], & |\tau| \le NT \\ 0, \quad \text{otherwise} \end{cases} \tag{2.3}$$

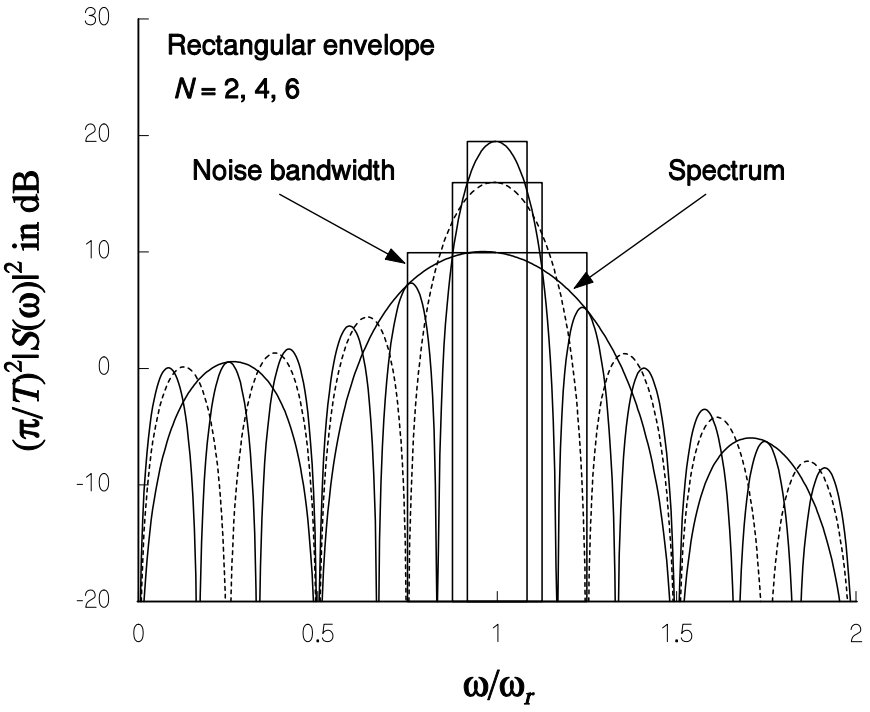

Figure 2.2 Illustration of noise bandwidth.

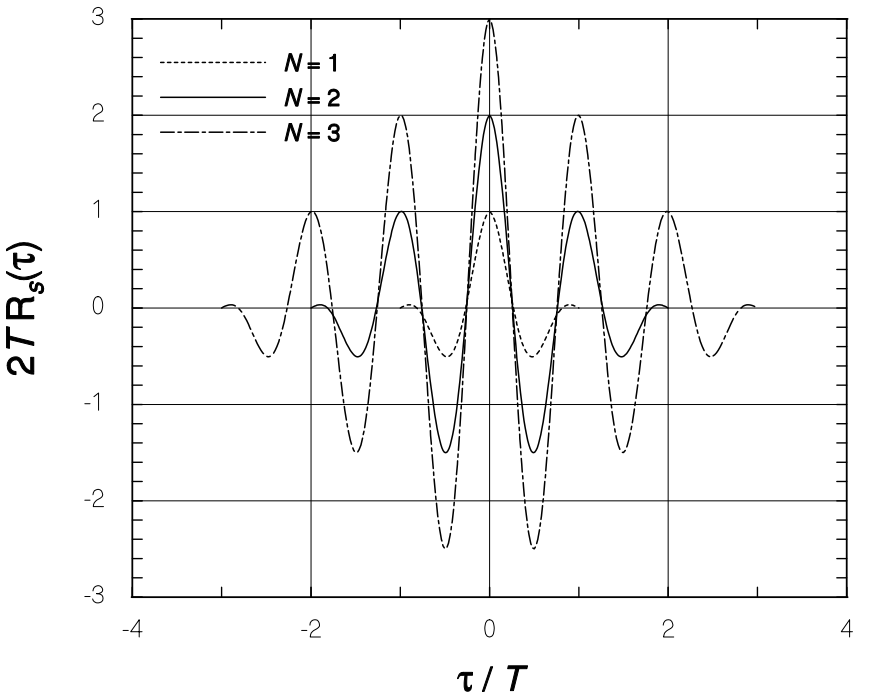

Figure 2.3 Polycycle autocorrelation function.

2.1.2 N-cycle Sinusoid with Triangular Envelope

Instead of a simple gated-on, gated-off sinusoidal model, one involving a linear-increase and a linear-decrease can be used. Because the tapered envelope guarantees that the waveform is continuous, it is possible to consider both a coherent model, for which the envelope timing is exactly related to that of the sinusoid, and a noncoherent model, for which the phase and frequency of the sinusoid are not necessarily related to the envelope.

2.1.2.1 Coherent Model

A coherent model for a sinusoidal burst with N cycles and a triangular envelope may be formulated as follows:

$$s(t) = \sin(\omega_r t)\left[\frac{4t}{NT}\,u(t) - \frac{8(t-NT/2)}{NT}\,u(t-NT/2) + \frac{4(t-NT)}{NT}\,u(t-NT)\right] \quad (2.4)$$

as shown for $N = 5$ and $N = 4.5$ in Figure 2.4. Note that the waveform has a central peak when $N = M + \frac{1}{2}$, where M is an integer. For N taking integer values, the Fourier transform of this waveform is given by

$$\begin{aligned} S(\omega) &= \frac{2j}{NT}\left\{\left[\frac{1-\mathrm{e}^{-j(\omega-\omega_r)NT/2}}{\omega-\omega_r}\right]^2 - \left[\frac{1-\mathrm{e}^{-j(\omega+\omega_r)NT/2}}{\omega+\omega_r}\right]^2\right\} \\ &= \frac{NT}{2j}\,\mathrm{e}^{-j\omega NT/2}\left[\mathrm{e}^{jN\pi}\,\mathrm{sinc}^2\left(\frac{(\omega-\omega_r)NT}{4\pi}\right) - \mathrm{e}^{-jN\pi}\,\mathrm{sinc}^2\left(\frac{(\omega+\omega_r)NT}{4\pi}\right)\right] \end{aligned} \quad (2.5a)$$

When N is an integer (giving a whole number of cycles under the envelope), the Fourier transform becomes

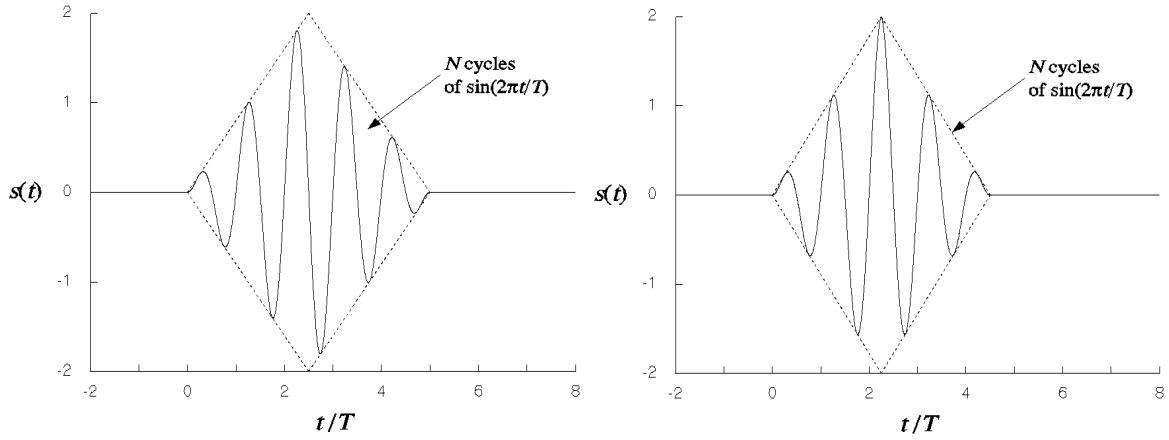

$N = 5$ $\qquad$ $N = 4.5$

Figure 2.4 Example N-cycle sinusoidal bursts with triangular pulse shaping.

$$S(\omega) = \left[1 - (-1)^N \mathrm{e}^{-j\omega NT/2}\right]^2 \frac{8j\omega/NT\omega_r^3}{\left[1 - (\omega/\omega_r)^2\right]^2}, \quad N \text{ an integer}$$

$$= \mathrm{e}^{-j\omega NT/2} \frac{32j\omega/NT\omega_r^3}{\left[1 - (\omega/\omega_r)^2\right]^2} \times \begin{cases} -\sin^2(N\omega T/4), & N \text{ an even integer} \\ \cos^2(N\omega T/4), & N \text{ an odd integer} \end{cases} \tag{2.5b}$$

For an odd number of half-cycles ($N = M + 1/2$), giving a waveform peak at its center point, the Fourier transform of the waveform is given by

$$S(\omega) = \frac{8\,\mathrm{e}^{-j\omega NT/2}}{NT} \cdot \frac{(-1)^M \left[1 + (\omega/\omega_r)^2\right] - 2(\omega/\omega_r)\sin(N\omega T/2)}{\omega_r^2 \left[1 - (\omega/\omega_r)^2\right]^2} \tag{2.5c}$$

Plots of the power spectra based on (2.5b) and (2.5c) are shown in Figure 2.5.

A general expression for the autocorrelation function of the waveform is given in Section A.1 of the Appendix. For reference, the autocorrelation function for N taking integer values is

$$\mathrm{R}_s(\tau) = \frac{NT}{2}\cos(\omega_r\tau)\left[\frac{4}{3} - \frac{8\tau^2}{(NT)^2} + \frac{8|\tau|^3}{(NT)^3} - 4\frac{1 - 3|\tau|/NT}{(2\pi N)^2}\right] - \frac{12NT}{(2\pi N)^3}\sin(\omega_r|\tau|)$$

$$0 \le |\tau| \le NT/2 \tag{2.6a}$$

$$= \frac{NT}{2}\cos(\omega_r\tau)\left[\frac{8}{3} - \frac{8|\tau|}{NT} + \frac{8\tau^2}{(NT)^2} - \frac{8|\tau|^3}{3(NT)^3} + 4\frac{1 - |\tau|/NT}{(2\pi N)^2}\right] + \frac{4NT}{(2\pi N)^3}\sin(\omega_r|\tau|)$$

$$NT/2 \le |\tau| \le NT \tag{2.6b}$$

This function is plotted in Figure 2.6 for $N = 1$ to 3. The autocorrelation function of the triangular-envelope polycycle for $N = M + \frac{1}{2}$, where M is an integer, is given by

$$\mathrm{R}_s(\tau) = \frac{NT}{2}\cos(\omega_r\tau)\left[\frac{4}{3} - \frac{8\tau^2}{(NT)^2} + \frac{8|\tau|^3}{(NT)^3} + 4\frac{1 - |\tau|/NT}{(2\pi N)^2}\right] + \frac{4NT}{(2\pi N)^3}\sin(\omega_r|\tau|)$$

$$0 \le |\tau| \le NT/2 \tag{2.7a}$$

$$= \frac{NT}{2}\cos(\omega_r\tau)\left[\frac{8}{3} - \frac{8|\tau|}{NT} + \frac{8\tau^2}{(NT)^2} - \frac{8|\tau|^3}{3(NT)^3} + 4\frac{1 - |\tau|/NT}{(2\pi N)^2}\right] + \frac{4NT}{(2\pi N)^3}\sin(\omega_r|\tau|)$$

$$NT/2 \le |\tau| \le NT \tag{2.7b}$$

This function is plotted in Figure 2.7 for $N = 1.5$ to 3.5.

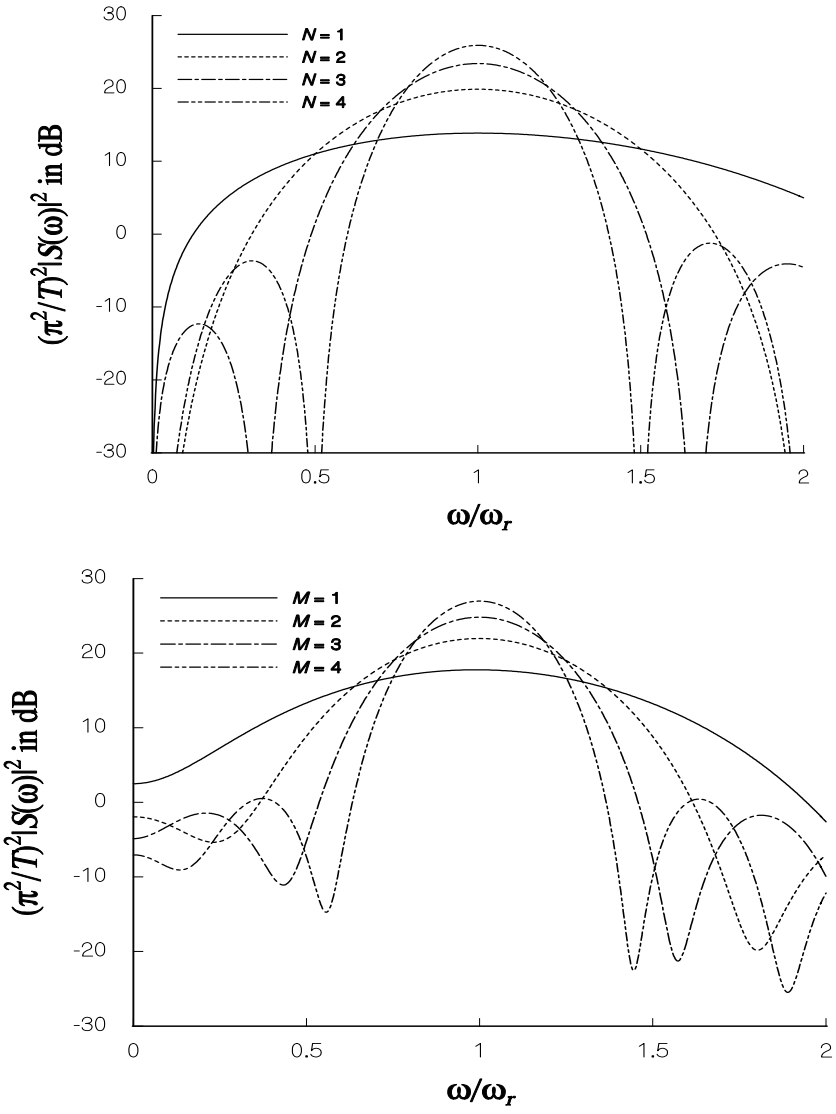

Figure 2.5 Power spectra for sinusoidal bursts with triangular pulse shaping.

.

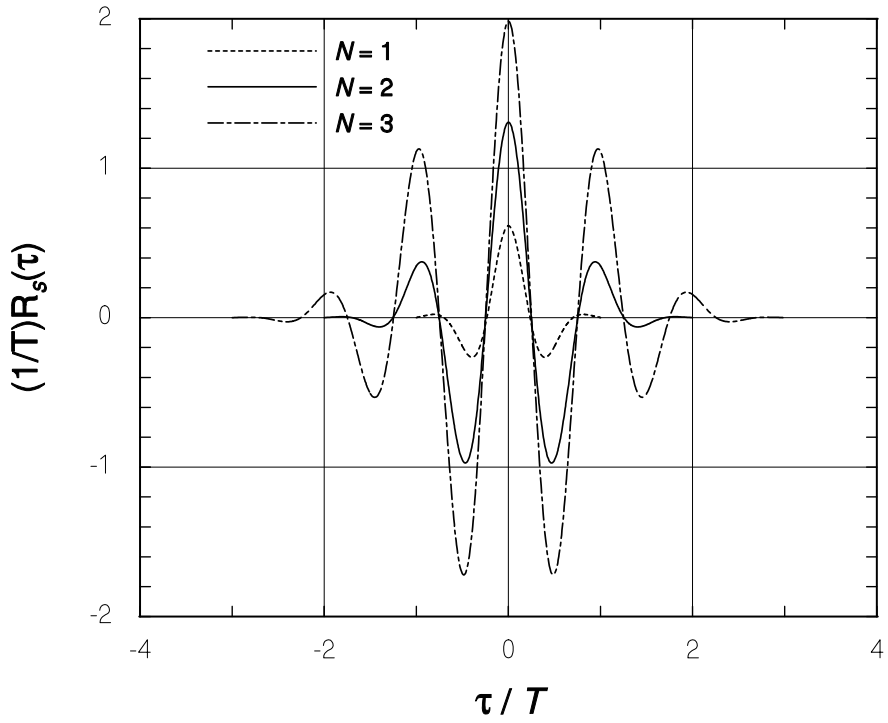

Figure 2.6 Autocorrelation function for sinusoidal bursts with triangular pulse shaping ($N = 1$, 2, and 3 cycles).

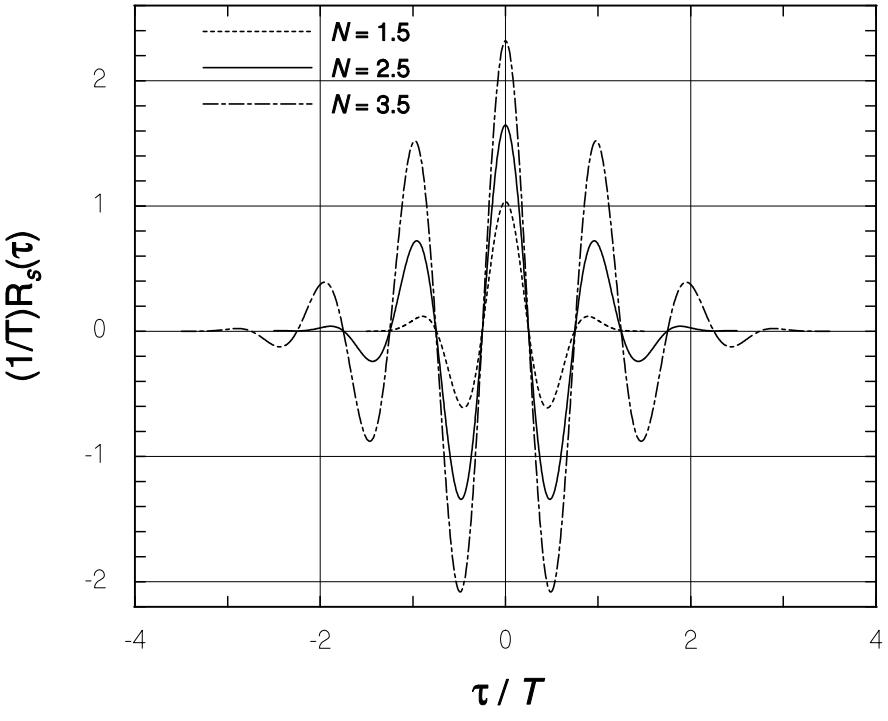

Figure 2.7 Autocorrelation function for sinusoidal bursts with triangular pulse shaping ($N = 1.5$, 2.5, and 3.5 cycles)

2.1.2.2 Noncoherent Model

A noncoherent model for a sinusoidal burst with N cycles and a triangular envelope may be formulated as follows:

$$s(t) = \sin(\omega_r t + \varphi)\left[\frac{4t}{NT}\,u(t) - \frac{8(t-NT/2)}{NT}\,u(t-NT/2) + \frac{4(t-NT)}{NT}\,u(t-NT)\right] \quad (2.8)$$

where φ is a random phase, uniformly distributed between 0 and 2π. For this case, we may calculate the autocorrelation function for the signal as an expected value/average:

$$\mathrm{R}_s(\tau) = \mathrm{E}\{s(t)s(t-\tau)\} = \tfrac{1}{2}\cos(\omega_r\tau) \times \overline{\mathrm{V}(t)\mathrm{V}(t-\tau)} \quad (2.9a)$$

where $\mathrm{V}(t)$ denotes the envelope. The envelope autocorrelation function is

$$\overline{\mathrm{V}(t)\mathrm{V}(t-\tau)} = \begin{cases} NT\left[\dfrac{4}{3} - \dfrac{8\tau^2}{(NT)^2} + \dfrac{8|\tau|^3}{(NT)^3}\right], & |\tau| \le NT/2 \\ 8NT\left[\dfrac{1}{3} - \dfrac{|\tau|}{NT} + \dfrac{\tau^2}{(NT)^2} - \dfrac{|\tau|^3}{3(NT)^3}\right], & NT/2 < |\tau| \le NT \end{cases} \quad (2.9b)$$

As shown in Figure 2.8, the autocorrelation function for the noncoherent model of the sinusoid with a triangular envelope is very similar to that for the coherent model as shown previously.

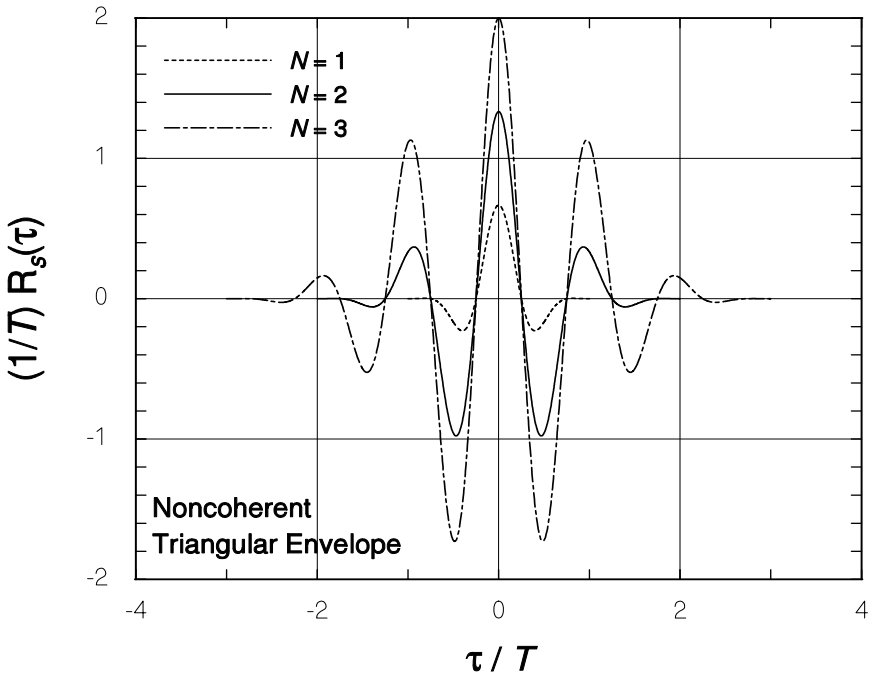

Figure 2.8 Autocorrelation function for noncoherent sinusoid with triangular envelope

The spectrum corresponding to the autocorrelation function in (2.9a) is given by its Fourier transform:

$$|S(\omega)|^2 = \mathrm{F}\{\mathrm{R}_s(\tau)\} = \frac{(NT)^2}{4}\left[\mathrm{sinc}^4\left(\frac{\omega-\omega_r}{4\pi}NT\right) + \mathrm{sinc}^4\left(\frac{\omega+\omega_r}{4\pi}NT\right)\right] \qquad (2.10a)$$

Examples of this spectrum are shown in Figure 2.9. The equivalent rectangular (noise) bandwidth of the bandpass signal, denoted B (in Hz), equals that of the envelope (modulation), which in this case is a triangular function, which has a $\mathrm{sinc}^4(\omega NT/4\pi)$ spectrum. Using formula 3.827.7 of [7], B is found to be

$$2\pi B = \int_{-\infty}^{\infty} d\omega\, \mathrm{sinc}^4\left(\frac{\omega}{4\pi}NT\right) = \frac{4}{NT}\int_{-\infty}^{\infty} dx\, \frac{\sin^4 x}{x^4} = \frac{8\pi}{3NT} = \frac{4}{3N}\omega_r \qquad (2.10b)$$

It is interesting to note that the 3-dB signal bandwidth, denoted B_3 (in Hz), is given by

$$0.5 = \mathrm{sinc}^4\left(\frac{NB_3T}{4}\right) \quad \Rightarrow \quad 2\pi B_3 = 0.319\,\frac{8\pi}{NT} = 1.276\,\frac{\omega_r}{N} \qquad (2.10c)$$

B_3 in this case is slightly smaller than the noise bandwidth, which equals the 3.3-dB bandwidth.

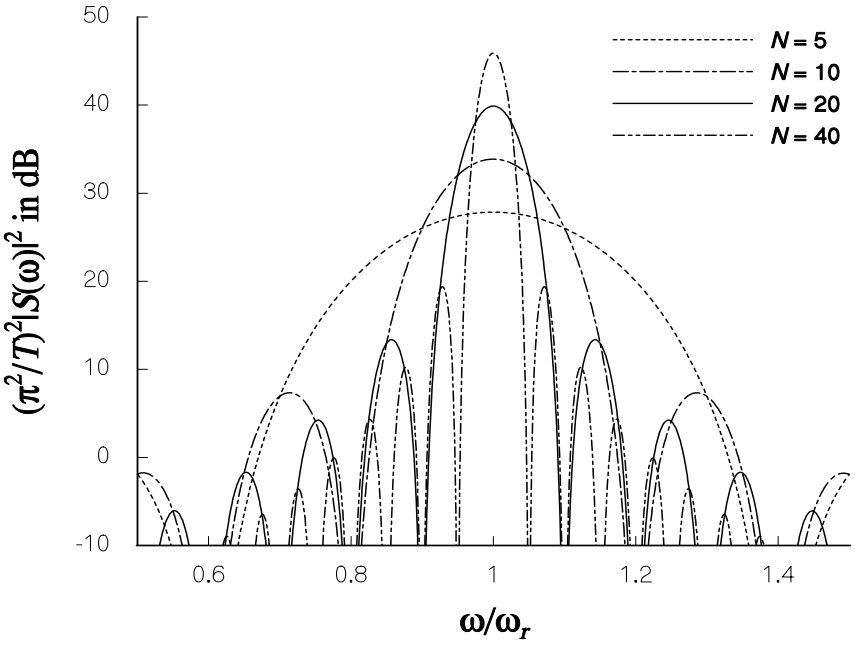

Figure 2.9 Spectra of noncoherent sinusoid with triangular envelope

2.1.3 N-cycle Sinusoid with Rectified Cosine Envelope

Another sinusoidal model, one involving "rectified cosine" envelope, has been proposed for UWB signals ([8], [9], [10]). Because the envelope guarantees that the waveform is continuous, it is possible to consider both a coherent model, for which the envelope timing is exactly related to that of the sinusoid, and a noncoherent model, for which the phase and frequency of the sinusoid are not necessarily related to the envelope.

2.1.3.1 Coherent Model

As illustrated in Figure 2.10, a coherent model for a sinusoidal burst with N cycles and a rectified cosine envelope may be formulated as follows:

$$s(t) = \cos(\omega_e t)\cos(\omega_r t), \quad |t| \le \pi/2\omega_e, \quad \omega_r = 2N\omega_e \tag{2.11}$$

where $T_e = 2\pi/\omega_e$ is the period of the envelope cosine (twice the pulse duration) and $T = 2\pi/\omega_r = \pi/N\omega_e$ is the period of the sinusoid. The Fourier transform of this signal model is given by

$$S(\omega) = \frac{\pi}{2\omega_e}\left\{\text{sinc}\left(\frac{\omega-(2N+1)\omega_e}{2\omega_e}\right) + \text{sinc}\left(\frac{\omega-(2N-1)\omega_e}{2\omega_e}\right) + \text{sinc}\left(\frac{\omega+(2N+1)\omega_e}{2\omega_e}\right) + \text{sinc}\left(\frac{\omega+(2N-1)\omega_e}{2\omega_e}\right)\right\} \tag{2.12a}$$

$$= \frac{(-1)^N T}{4\pi N}\cos\left(N\pi\frac{\omega}{\omega_r}\right)\left\{\left[\frac{1}{4N^2} - \left(\frac{\omega}{\omega_r}+1\right)^2\right]^{-1} + \left[\frac{1}{4N^2} - \left(\frac{\omega}{\omega_r}-1\right)^2\right]^{-1}\right\} \tag{2.12b}$$

Examples of the spectrum related to $S(\omega)$ are shown in Figure 2.11.

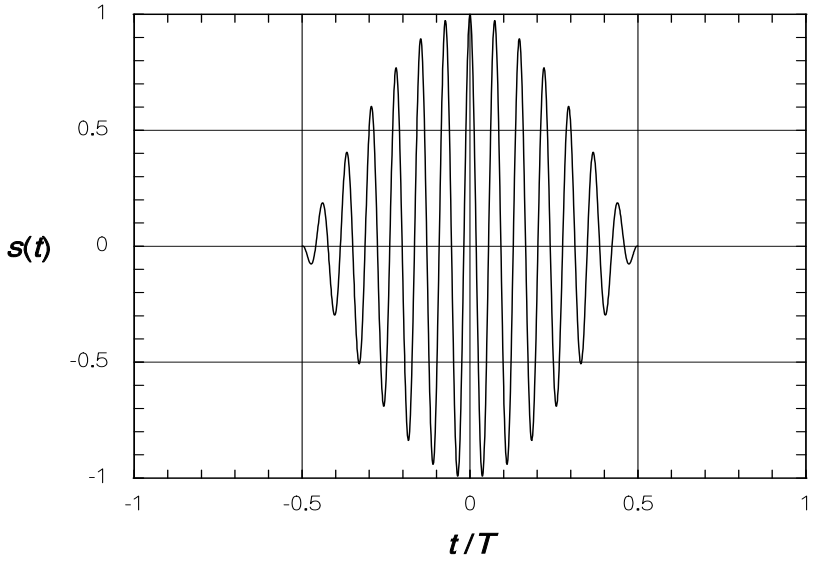

Figure 2.10 Sinusoid with cosine envelope.

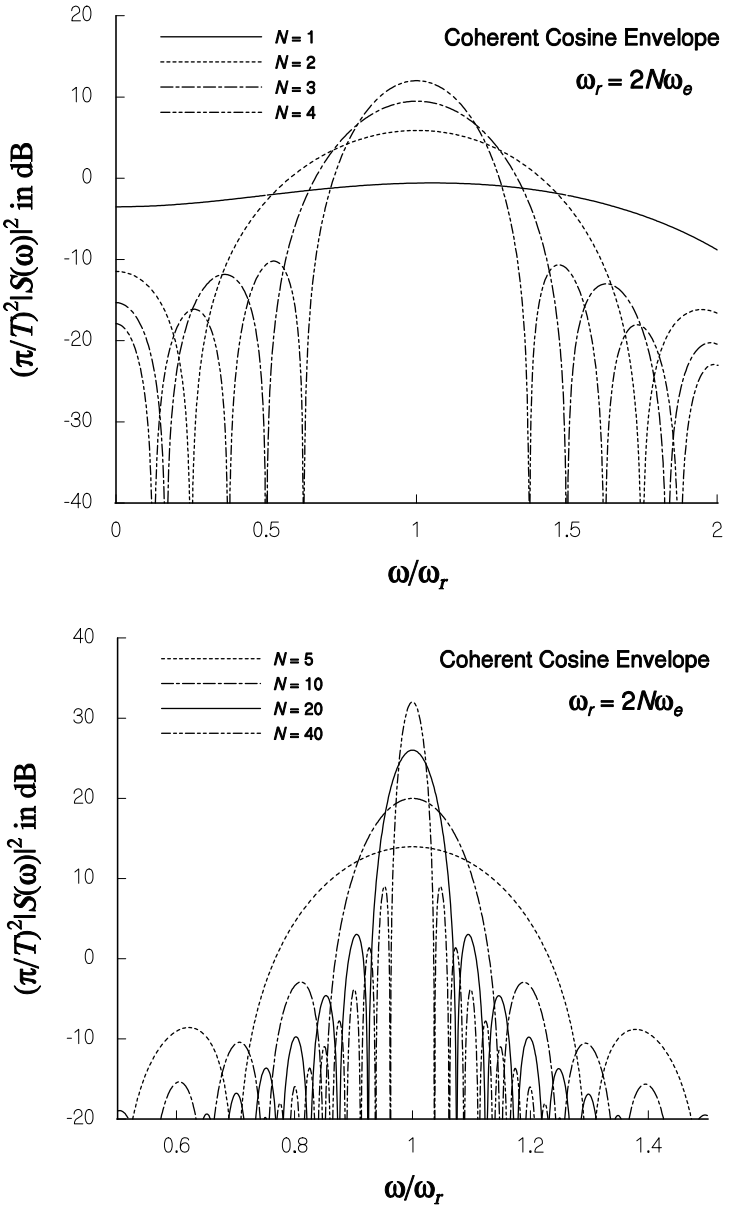

Figure 2.11 Spectra of coherent sinusoid with rectified cosine envelope

The autocorrelation function for the waveform in (2.11) is found to be

$$\mathrm{R}_s(\tau) = \frac{1}{4}\left(\frac{\pi}{\omega_e} - |\tau|\right)\cos(\omega_e\tau)\cos(\omega_r\tau) + \frac{1}{8}\,\frac{\sin[(2N+1)\omega_e|\tau|]}{(2N+1)\omega_e} + \frac{1}{8}\,\frac{\sin[(2N-1)\omega_e|\tau|]}{(2N-1)\omega_e}$$
$$+ \frac{1}{4}\cos(\omega_r\tau)\frac{\sin(\omega_e|\tau|)}{\omega_e} - \frac{1}{4}\cos(\omega_e\tau)\frac{\sin(\omega_r|\tau|)}{\omega_r} \qquad (2.13)$$

Examples of this autocorrelation function are shown in Figure 2.12.

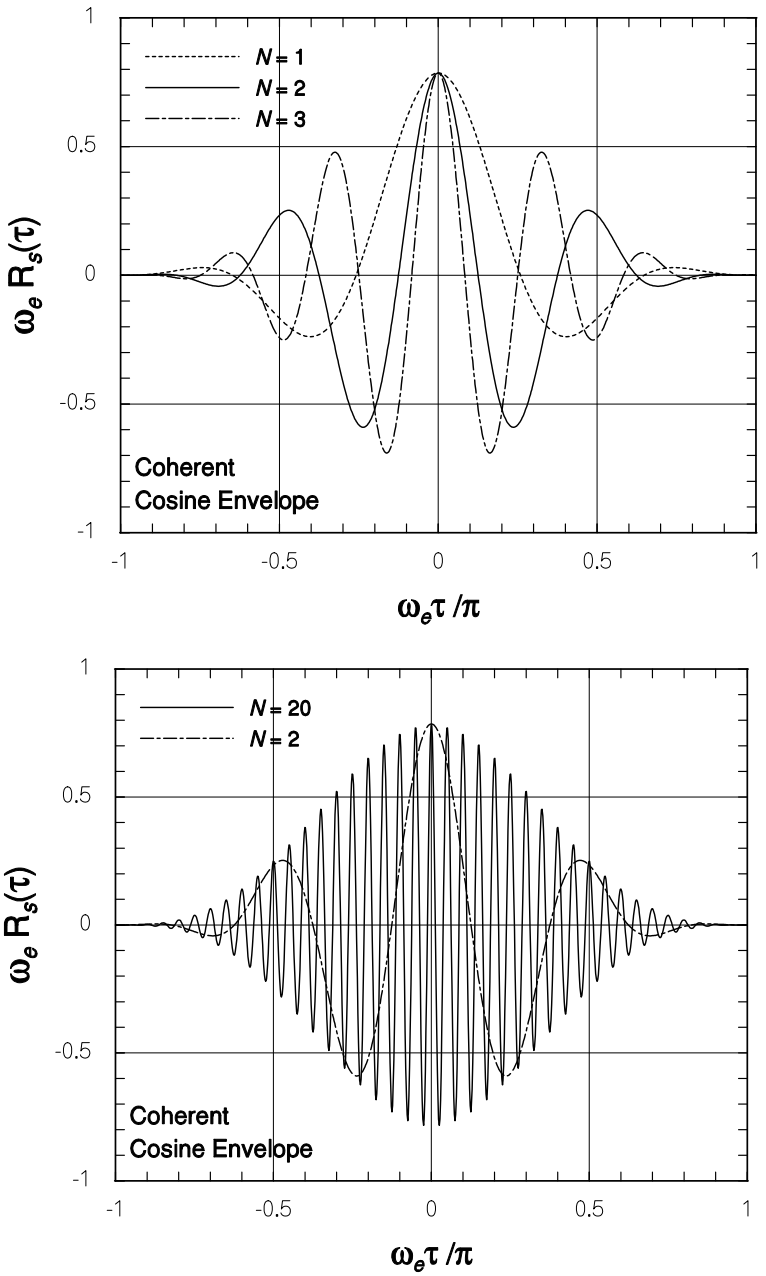

Figure 2.12 Autocorrelation function of sinusoid with rectified cosine envelope.

2.1.3.2 Noncoherent Model

A noncoherent model for a sinusoidal burst with N cycles and a rectified cosine envelope may be formulated as follows:

$$s(t) = \cos(\omega_e t)\cos(\omega_r t + \varphi), \quad |t| \leq \pi/2\omega_e, \quad \omega_r = 2N\omega_e \tag{2.14}$$

where φ is a random phase, uniformly distributed between 0 and 2π. For this case, we may calculate the autocorrelation function for the signal as an expected value/average:

$$\mathrm{R}_s(\tau) = \mathrm{E}\{s(t)s(t-\tau)\} = \tfrac{1}{2}\cos(\omega_r\tau) \times \overline{\mathrm{V}(t)\mathrm{V}(t-\tau)} \tag{2.15a}$$

where $\mathrm{V}(t)$ denotes the envelope. The envelope autocorrelation function is

$$\overline{\mathrm{V}(t)\mathrm{V}(t-\tau)} = \mathrm{R}_V(\tau) = \frac{1}{2}\left(\frac{\pi}{\omega_e} - |\tau|\right)\cos(\omega_e\tau) + \frac{\sin(\omega_e|\tau|)}{2\omega_e}, \quad |\tau| \le \frac{\pi}{\omega_e} \tag{2.15b}$$

and the corresponding spectrum is

$$|S_V(\omega)|^2 = \left[\frac{\sin\Big((\omega-\omega_e)\,\pi/2\omega_e\Big)}{\omega-\omega_e} + \frac{\sin\Big((\omega+\omega_e)\,\pi/2\omega_e\Big)}{\omega+\omega_e}\right]^2 \tag{2.15c}$$

Examples of the autocorrelation function in (2.15a) are shown in Figure 2.13. For $N > 1$, there is very little difference between the autocorrelation functions for the coherent and noncoherent sinusoids with a rectified cosine envelope.

The spectrum corresponding to (2.15a) and (2.15b) is found to be

$$|S(\omega)|^2 = \frac{1}{2}\left\{\left[\frac{\sin\left(\dfrac{\omega-\omega_e-\omega_r}{2\omega_e}\pi\right)}{\omega-\omega_e-\omega_r} + \frac{\sin\left(\dfrac{\omega+\omega_e-\omega_r}{2\omega_e}\pi\right)}{\omega+\omega_e-\omega_r}\right]^2 + \left[\frac{\sin\left(\dfrac{\omega-\omega_e+\omega_r}{2\omega_e}\pi\right)}{\omega-\omega_e+\omega_r} + \frac{\sin\left(\dfrac{\omega+\omega_e+\omega_r}{2\omega_e}\pi\right)}{\omega+\omega_e+\omega_r}\right]^2\right\} \tag{2.16a}$$

$$= \frac{T^2}{16N^2\pi^2}\cos^2\left(\frac{\omega}{\omega_r}N\pi\right)\left\{\left[\left(\frac{\omega}{\omega_r}+1\right)^2 - \frac{1}{4N^2}\right]^{-2} + \left[\left(\frac{\omega}{\omega_r}-1\right)^2 - \frac{1}{4N^2}\right]^{-2}\right\} \tag{2.16b}$$

An example of this spectrum is shown in Figure 2.14. The equivalent rectangular (noise) bandwidth of the bandpass signal, denoted B (in Hz), equals that of the envelope (modulation), which in this case is a cosine function with the spectrum in (2.15c). B is found from

$$2\pi B \cdot |S_V(0)|^2 = \int_{-\infty}^{\infty} d\omega\, |S_V(\omega)|^2 = 2\pi\,\mathrm{R}_V(0) \quad \Rightarrow \quad 2\pi B = \frac{\pi^2}{4}\,\omega_e = \frac{\pi^2}{8}\,\frac{\omega_r}{N} \tag{2.16c}$$

The 3-dB signal bandwidth, denoted B_3 (in Hz), is given by

$$0.5 = |S_V(\pi B_3)|^2 / |S_V(0)|^2 \quad \Rightarrow \quad 2\pi B_3 = 2.378\,\omega_e = 1.189\,\frac{\omega_r}{N} \tag{2.16d}$$

B_3 in this case is slightly smaller than the noise bandwidth, which equals the 3.25-dB bandwidth.

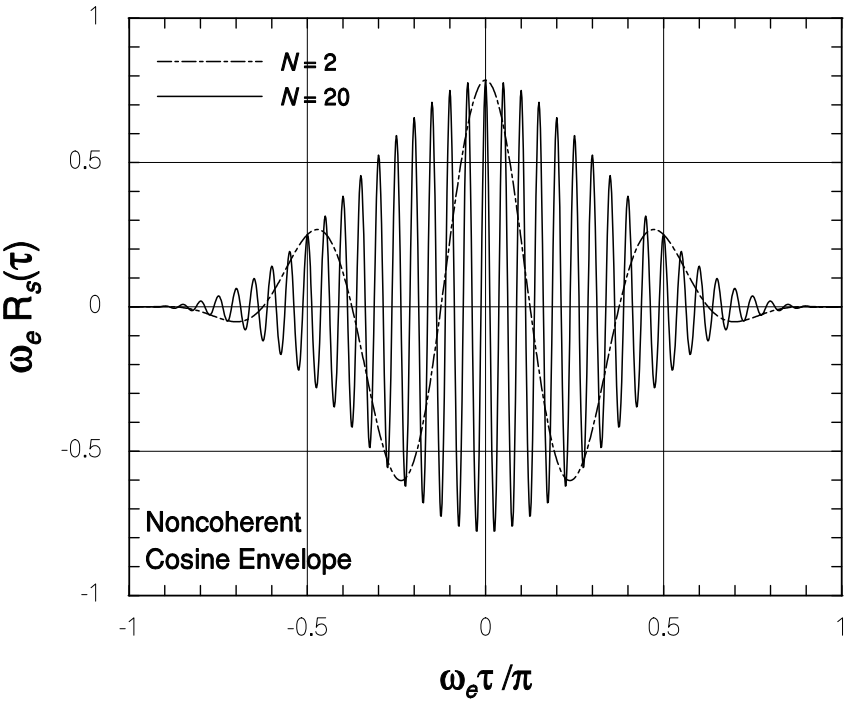

Figure 2.13 Autocorrelation function for noncoherent sinusoid with rectified cosine envelope.

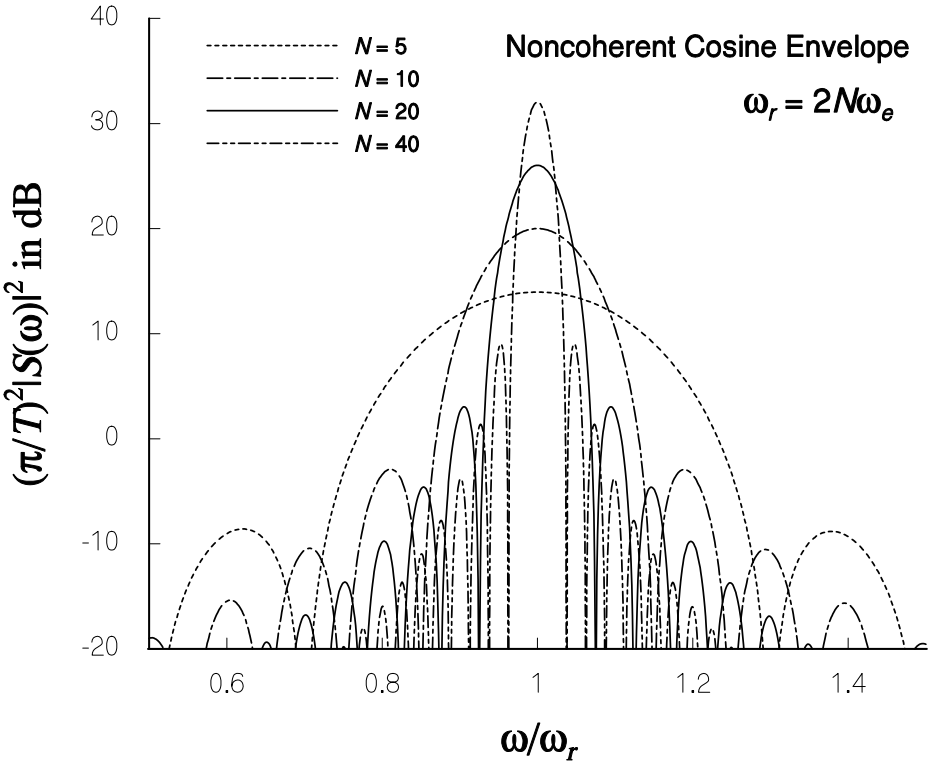

Figure 2.14 Spectrum for noncoherent sinusoid with rectified cosine envelope.

2.2 Sinusoid with Gaussian Envelope

Another sinusoidal model, one involving a Gaussian envelope, has been proposed for UWB signals ([11], [12], [13]). Because the envelope guarantees that the waveform is continuous, it is possible to consider both a coherent model, for which the envelope timing is exactly related to that of the sinusoid, and a noncoherent model, for which the phase and frequency of the sinusoid are not necessarily related to the envelope.

2.2.1 Coherent Model

A coherent model for a sinusoidal burst with a Gaussian envelope, illustrated in Figure 2.15, may be formulated as follows:

$$s(t) = \mathrm{e}^{-at^2}\cos(\omega_r t) \tag{2.17}$$

The autocorrelation function and corresponding spectrum for this signal model are

$$\mathrm{R}_s(\tau) = \frac{1}{2}\sqrt{\frac{\pi}{2a}}\,\mathrm{e}^{-a\tau^2/2}\left[\cos(\omega_r\tau) + \mathrm{e}^{-\omega_r^2/2a}\right] \tag{2.18}$$

$$|S(\omega)|^2 = \frac{\pi}{4a}\left[\mathrm{e}^{-(\omega-\omega_r)^2/4a} + \mathrm{e}^{-(\omega+\omega_r)^2/4a}\right]^2 \tag{2.19}$$

Plots of the autocorrelation function and spectrum are shown in Figures 2.16 and 2.17, respectively.

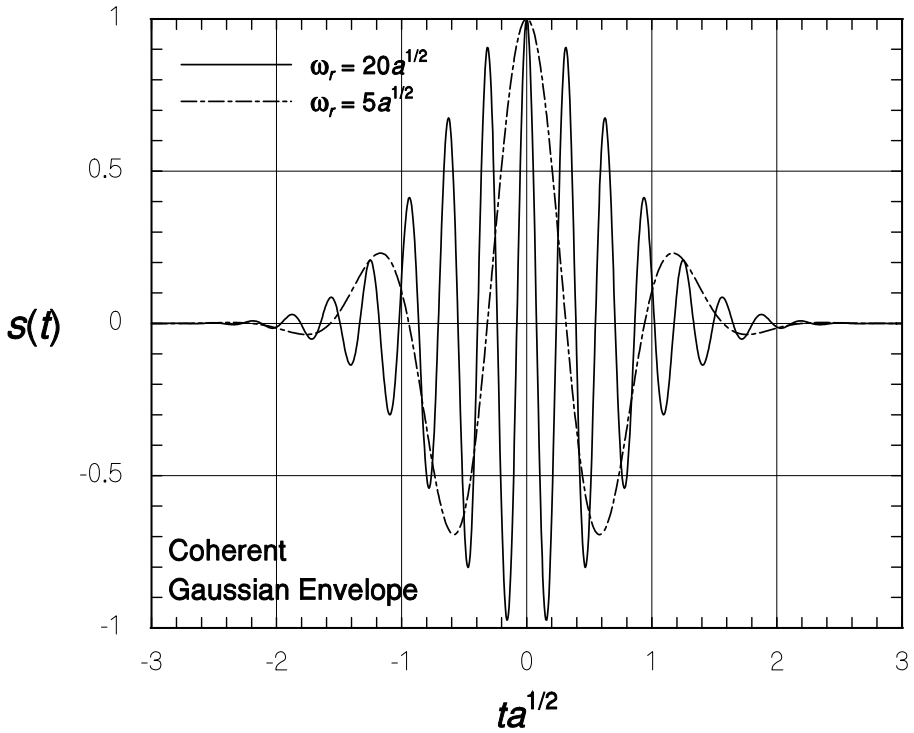

Figure 2.15 Sinusoid with Gaussian envelope.

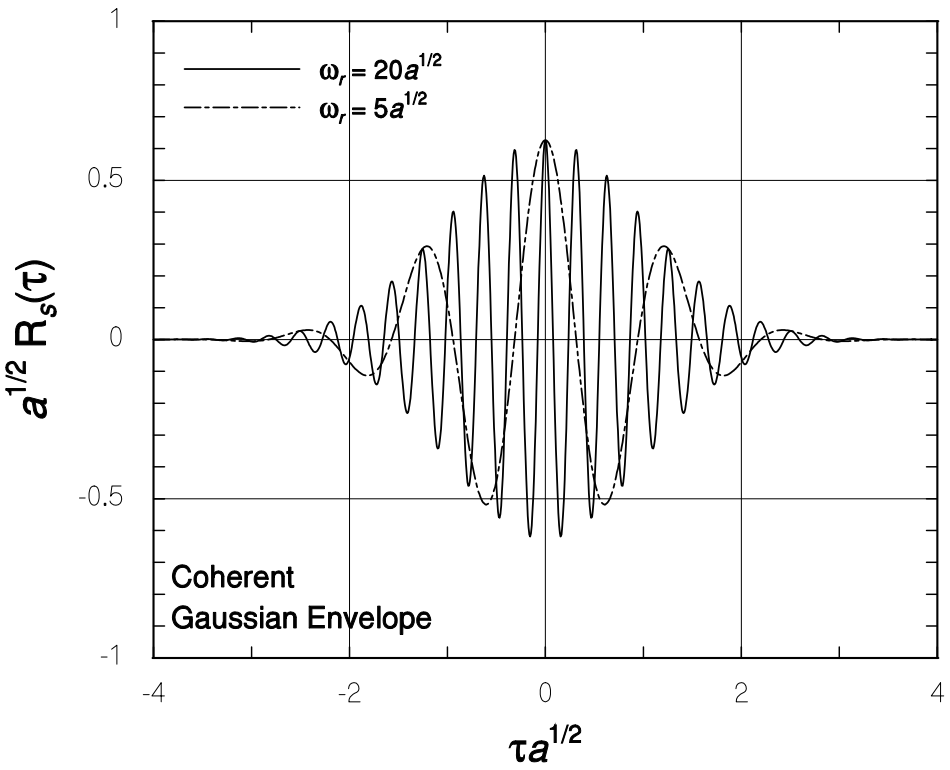

Figure 2.16 Autocorrelation function for coherent sinusoid with Gaussian envelope.

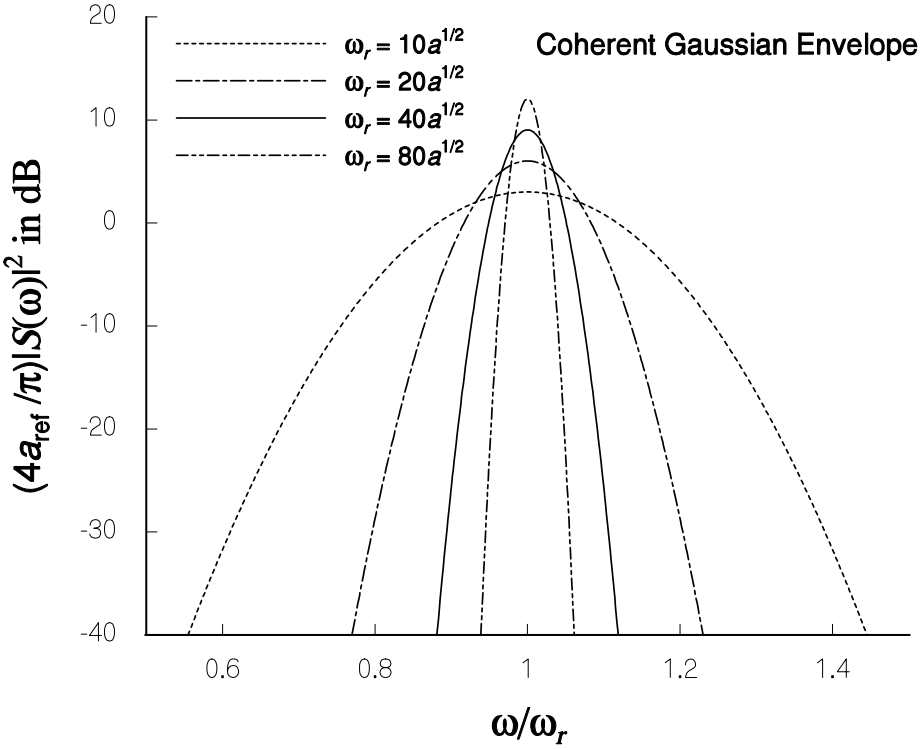

Figure 2.17 Spectra of coherent sinusoid with Gaussian envelope.

Perhaps the most significant feature of the sinusoid with a Gaussian pulse shape is that the spectrum has no sidelobes at all.

2.2.2 Noncoherent Model

A noncoherent model for a sinusoidal burst with a Gaussian envelope may be formulated as follows:

$$s(t) = \mathrm{e}^{-at^2}\cos(\omega_r t + \varphi) \tag{2.20}$$

where φ is a random phase, uniformly distributed between 0 and 2π. For this case, we may calculate the autocorrelation function for the signal as an expected value/average:

$$\mathrm{R}_s(\tau) = \mathrm{E}\{s(t)s(t-\tau)\} = \tfrac{1}{2}\cos(\omega_r\tau) \times \overline{\mathrm{V}(t)\mathrm{V}(t-\tau)} \tag{2.21a}$$

where $\mathrm{V}(t)$ denotes the envelope, whose autocorrelation function is given by

$$\overline{\mathrm{V}(t)\mathrm{V}(t-\tau)} = \mathrm{R}_V(\tau) = \int_{-\infty}^{\infty} dt\, \mathrm{e}^{-at^2}\mathrm{e}^{-a(t-\tau)^2} = \mathrm{e}^{-a\tau^2/2}\sqrt{\frac{\pi}{2a}} \tag{2.21b}$$

The spectrum corresponding to this autocorrelation function is

$$|S(\omega)|^2 = \frac{\pi}{4a}\left[\mathrm{e}^{-(\omega-\omega_r)^2/2a} + \mathrm{e}^{-(\omega+\omega_r)^2/2a}\right] \tag{2.22a}$$

To the degree of precision reflected in the plots, Figures 2.16 and 2.17, respectively, represent the autocorrelation function and spectrum in (2.21) and (2.22). The equivalent rectangular (noise) bandwidth of the bandpass signal, denoted B (in Hz), equals that of the envelope (modulation), which in this case is a Gaussian pulse. B is found from

$$2\pi B \cdot |S_V(0)|^2 = \int_{-\infty}^{\infty} d\omega\, |S_V(\omega)|^2 = 2\pi\, \mathrm{R}_V(0) \;\Rightarrow\; 2\pi B = \sqrt{2\pi a} \tag{2.22b}$$

or $a = 2\pi B^2$. The 3-dB signal bandwidth, denoted B_3 (in Hz), is given by

$$0.5 = |S_V(\pi B_3)|^2/|S_V(0)|^2 \quad \Rightarrow \quad 2\pi B_3 = 2\sqrt{(2\,ln2)a} \tag{2.22c}$$

B_3 in this case is slightly smaller than the noise bandwidth, which equals the 3.41-dB bandwidth.

2.3 Hermite Polynomial Model

Another mathematical model for UWB pulses is based on the resemblance of the so-called Gaussian pulse shape to a monopulse and the fact that its nth derivative has n zero crossings [14]. The derivatives can be expressed in terms of the original monopulse using Hermite polynomials, as shown in the following equations:

Hermite polynomials [15]: $$He_n(t) = \mathrm{e}^{x^2/2}\,(-1)^n\,\frac{d^n}{dx^n}\left(\mathrm{e}^{-x^2/2}\right) \tag{2.23a}$$

where

$$He_0(x) = 1,\ He_1(x) = x,\ He_{n+1}(x) = x\,He_n(x) - n\,He_{n-1}(x) \tag{2.23b}$$

A model UWB pulse shape based on these concepts is [14]

$$s_n(t) = \mathrm{e}^{-t^2/4}\,He_n(t) = \mathrm{e}^{t^2/4}\,(-1)^n\,\frac{d^n}{dt^n}\left(\mathrm{e}^{-t^2/2}\right) \tag{2.24a}$$

or its parameterized version [4]

$$p_n(t) = s_n(t/T) \tag{2.24b}$$

where T is a convenient measure of pulse width. The recurrence relation in (2.23b) can be applied directly to $s_n(t)$, and it is straightforward to show that the Fourier transform of $s_n(t)$ is given by

$$S_n(\omega) = \mathcal{F}\{s_n(t)\} = 2\sqrt{\pi}\,\mathrm{e}^{-\omega^2}\,(-j)^n He_n(2\omega) \tag{2.25a}$$

with the recurrence relations

$$S_{n+1}(\omega) = -2j\omega\,S_n(\omega) + n\,S_{n-1}(\omega) \tag{2.25b}$$

$$S_0(\omega) = 2\sqrt{\pi}\,\mathrm{e}^{-\omega^2},\ \ S_1(\omega) = -4j\omega\sqrt{\pi}\,\mathrm{e}^{-\omega^2} \tag{2.25c}$$

Examples of $s_n(t)$ and of power spectra based on $S_n(\omega)$ are shown in Figures 2.18 and 2.19, respectively. Note in Figure 2.18 that increasing n not only increases the number of zero-crossings (half-cycles by analogy with the polycycle waveforms discussed previously) but also the duration of the overall waveform. The apparent periods of the oscillations in Figure 2.18 are approximately T_n = (6.0, 5.6, 4.6, 3.8, 3.2, 2.8) for n = (0, 1, 2, 3, 4, 5), respectively. The angular frequency in Figure 2.19 is shown without normalization in part (a) of the figure, and in part (b) it is normalized (scaled) by the apparent angular frequency $\omega_n = 2\pi/T_n$ in Figure 2.19 for each value of n. Similar to the spectra for polycycle waveforms in Figure 2.1, the normalization in part (b) of Figure 2.19 shows Hermite polynomial-based waveforms' spectra becoming narrower about the center frequency of $\omega = \omega_n$; however, it is clear from this figure that these waveforms are far from ideal because in addition to the central peaks in the spectra there are large sidelobes.

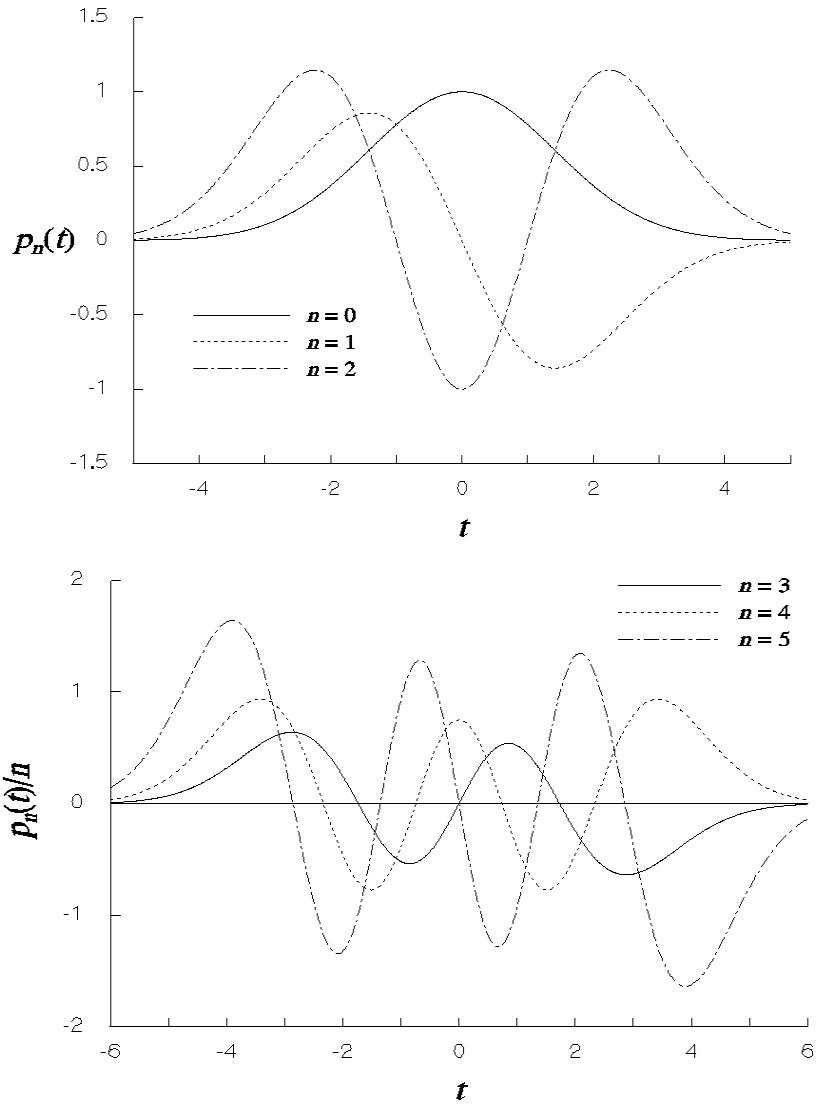

Figure 2.18 Example UWB waveforms based on Hermite polynomials.

It is shown in Appendix A.2 that the autocorrelation function for $s_n(t)$ has the following recursion:

$$\mathrm{R}_s(\tau;\, n+1) = (2n + 1 - \tau^2/4)\,\mathrm{R}_s(\tau;\, n) - n^2\,\mathrm{R}_s(\tau;\, n-1) \tag{2.11a}$$

with $$\mathrm{R}_s(\tau;\, 0) = \sqrt{2\pi}\,\mathrm{e}^{-\tau^2/8} \text{ and } \mathrm{R}_s(\tau;\, 1) = \sqrt{2\pi}\,\mathrm{e}^{-\tau^2/8}\left(1 - \tau^2/4\right) \tag{2.11b}$$

Plots of the autocorrelation function are shown in Figure 2.20 for $n = 0$ to $n = 4$.

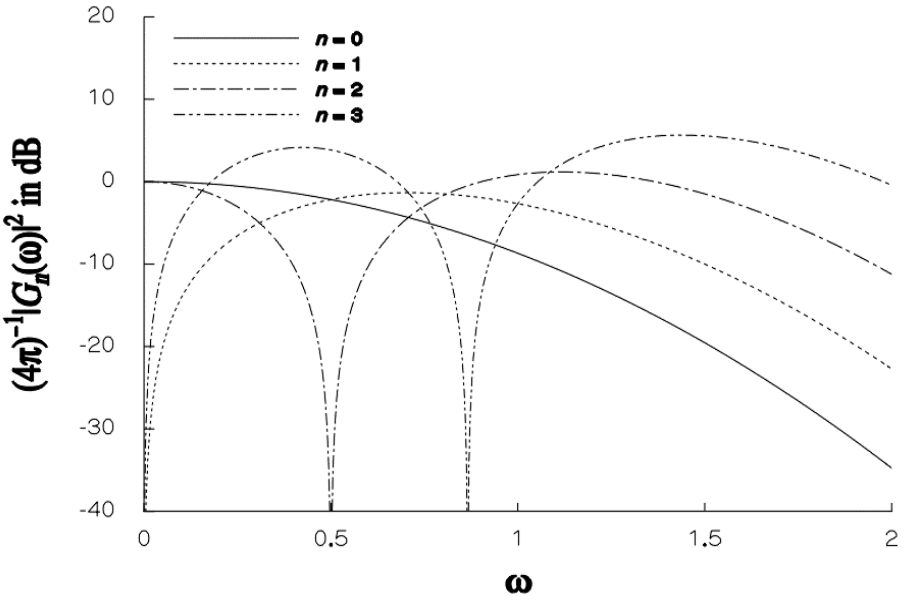

(a) Without normalization of the angular frequency

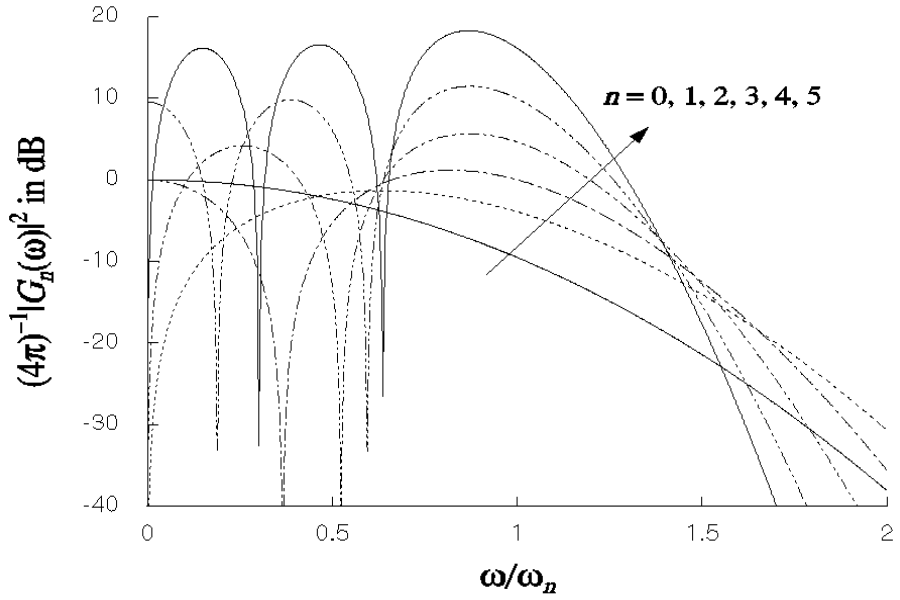

(b) With normalization of the angular frequency by the apparent angular frequency of the oscillations.

Figure 2.19 Power spectra for UWB pulses based on Hermite polynomials.

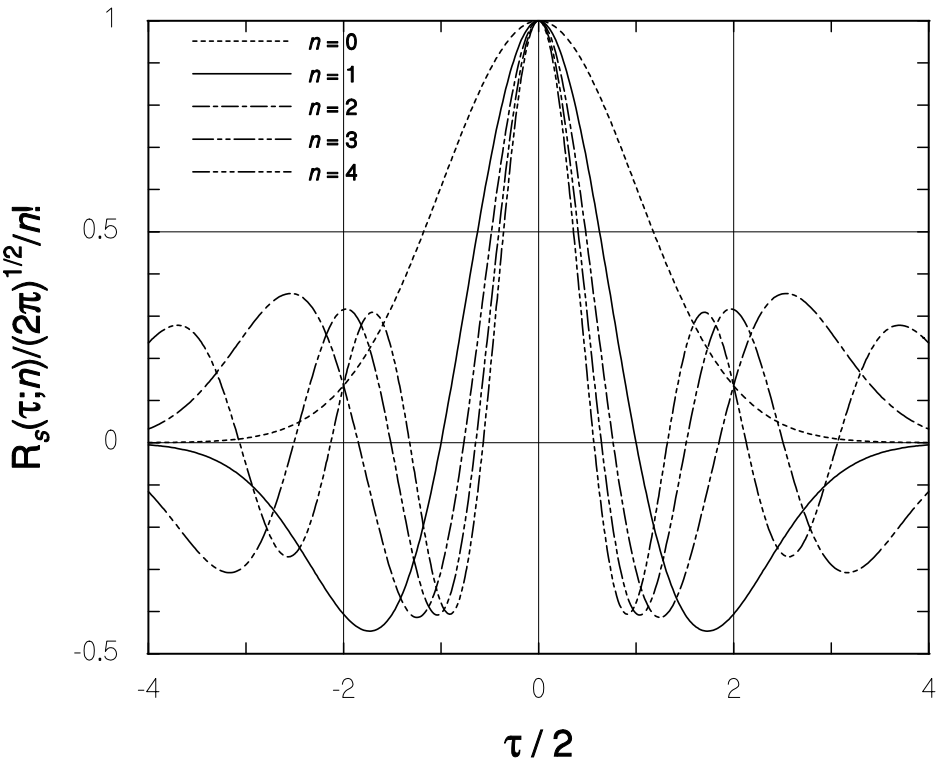

Figure 2.20 Autocorrelation function for Hermite polynomial pulse model.

APPENDIX

A.1 Autocorrelation Function for the N-cycle Sinusoid with Triangular Envelope

For $0 \le \tau \le NT/2$, the autocorrelation function for the N-cycle sinusoidal waveform model with a triangular envelope is given by

$$\begin{aligned}
\mathrm{R}_s(\tau) = \left(\frac{4}{NT}\right)^2 \Bigg\{ & \int_{\tau}^{NT/2} dt\, t(t-\tau)\sin(\omega_r t)\sin[\omega_r(t-\tau)] \\
& + \int_{NT/2}^{\tau+NT/2} dt\, (NT-t)(t-\tau)\sin(\omega_r t)\sin[\omega_r(t-\tau)] \\
& + \int_{\tau+NT/2}^{NT} dt\, (NT-t)(NT+\tau-t)\sin(\omega_r t)\sin[\omega_r(t-\tau)] \Bigg\} \\
= \left(\frac{4}{NT}\right)^2 \Bigg\{ & \frac{1}{2}\cos(\omega_r\tau)\left[\frac{(NT)^3}{12} - \frac{NT\tau^2}{2} + \frac{\tau^3}{2}\right] \\
& - \cos(\omega_r NT)\left[\frac{NT-2\tau}{4\omega_r^2}\cos(\omega_r\tau) + \frac{1}{2\omega_r^3}\sin(\omega_r\tau)\right] \\
& + \cos(\omega_r NT)\left[\frac{\tau}{4\omega_r^2}\cos[\omega_r(NT-\tau)] + \frac{1}{4\omega_r^3}\sin[\omega_r(NT-\tau)]\right] \Bigg\} \qquad \text{(A.1.1)}
\end{aligned}$$

For $NT/2 \le \tau \le NT$, the autocorrelation function is found to be

$$\begin{aligned}
\mathrm{R}_s(\tau) = \left(\frac{4}{NT}\right)^2 & \int_{\tau}^{NT} dt\, (NT-t)(t-\tau)\sin(\omega_r t)\sin[\omega_r(t-\tau)] \Bigg\} \\
= \left(\frac{4}{NT}\right)^2 \Bigg\{ & \frac{1}{2}\cos(\omega_r\tau)\left[\frac{(NT)^3}{6} - \frac{(NT)^2\tau}{2} + \frac{NT\tau^2}{2} - \frac{\tau^3}{6}\right] \\
& + \cos(\omega_r NT)\left[\frac{NT-\tau}{4\omega_r^2}\cos[\omega_r(NT-\tau)] - \frac{1}{4\omega_r^3}\sin[\omega_r(NT-\tau)]\right] \Bigg\} \qquad \text{(A.1.2)}
\end{aligned}$$

A.2 Autocorrelation Function for the Hermite Polynomial Model [17]

Using the notation $\eta = \tau/2$ for convenience, the autocorrelation function for the Hermite polynomial waveform model is given by

$$\mathrm{R}_s(\tau;\, n) = \int_{-\infty}^{\infty} dt\, s_n(t)\, s_n(t-\tau) = \int_{-\infty}^{\infty} dt\, s_n(t+\eta)\, s_n(t-\eta)$$

$$= \int_{-\infty}^{\infty} dt\, \mathrm{e}^{-(t+\eta)^2/4}\, He_n(t+\eta)\, \mathrm{e}^{-(t-\eta)^2/4} He_n(t-\eta)$$

$$= \mathrm{e}^{-\eta^2/2} \int_{-\infty}^{\infty} dt\, \mathrm{e}^{-t^2/2} He_n(t+\eta)\, He_n(t-\eta)$$

$$= \sqrt{2\pi}\, \mathrm{e}^{-\eta^2/2}\, \mathrm{E}_t\{He_n(t+\eta)\, He_n(t-\eta)\} \tag{A.2.1}$$

where E_t denotes expectation as if t is a zero-mean, unit-variance Gaussian random variable. For $n = 0$ to 4, we obtain by direct calculation

$$\mathrm{R}_s(\tau;\, 0) = \sqrt{2\pi}\, \mathrm{e}^{-\eta^2/2}\, \mathrm{E}_t\{1\} = \sqrt{2\pi}\, \mathrm{e}^{-\eta^2/2} \tag{A.2.3}$$

$$\mathrm{R}_s(\tau;\, 1) = \sqrt{2\pi}\, \mathrm{e}^{-\eta^2/2}\, \mathrm{E}_t\{t^2 - \eta^2\} = \sqrt{2\pi}\, \mathrm{e}^{-\eta^2/2}(1 - \eta^2) \tag{A.2.4}$$

$$\mathrm{R}_s(\tau;\, 2) = \sqrt{2\pi}\, \mathrm{e}^{-\eta^2/2}\, \mathrm{E}_t\{t^4 - 2t^2(\eta^2 + 1) + \eta^4 - 2\eta^2 + 1\} \tag{A.2.5a}$$

$$= \sqrt{2\pi}\, \mathrm{e}^{-\eta^2/2}(2 - 4\eta^2 + \eta^4) \tag{A.2.5b}$$

$$\mathrm{R}_s(\tau;\, 3) = \sqrt{2\pi}\, \mathrm{e}^{-\eta^2/2}\, \mathrm{E}_t\{t^6 - 3\,t^4(\eta^2 + 2) + 3\,t^2(\eta^4 + 3) - \eta^6 + 6\eta^4 - 9\eta^2\} \tag{A.2.6a}$$

$$= \sqrt{2\pi}\, \mathrm{e}^{-\eta^2/2}(6 - 18\eta^2 + 9\eta^4 - \eta^6) \tag{A.2.6b}$$

$$\mathrm{R}_s(\tau;\, 4) = \sqrt{2\pi}\, \mathrm{e}^{-\eta^2/2}\, \mathrm{E}_t\{t^8 - 4t^6(\eta^2 + 3) + 6t^4(\eta^4 + 2\eta^2 + 7) - 4t^2(\eta^6 - 3\eta^4 + 9\eta^2 + 9) + \eta^8 - 12\eta^6 + 42\eta^4 - 36\eta^2 + 9\} \tag{A.2.7a}$$

$$= \sqrt{2\pi}\, \mathrm{e}^{-\eta^2/2}(24 - 96\eta^2 + 72\eta^4 - 16\eta^6 + \eta^8) \tag{A.2.7b}$$

By inspection, the general form for these correlation functions is

$$\mathrm{R}_s(\tau;\, n) = \sqrt{2\pi}\, \mathrm{e}^{-\eta^2/2} \sum_{k=0}^{n} \frac{n!}{k!} \binom{n}{k} (-1)^k \eta^{2k} \tag{A.2.8a}$$

$$= \sqrt{2\pi}\, \mathrm{e}^{-\eta^2/2}\, n! \sum_{n=0}^{\infty} \frac{{\eta^2}^k}{k!} \frac{(-n)_k}{(1)_k} = \sqrt{2\pi}\, \mathrm{e}^{-\eta^2/2}\, n!\ {}_1\mathrm{F}_1(-n;\, 1;\, \eta^2) \tag{A.2.8b}$$

where ${}_1\mathrm{F}_1(a;\, b;\, x)$ denotes the confluent hypergeometric function and $(a)_k = \Gamma(a+k)/\Gamma(a)$ is Pochhammer's symbol. We may use Kummer's transformation [16, §13.1.27] to write

$${}_1\mathrm{F}_1(-n;\, 1;\, \eta^2) = \mathrm{e}^{\eta^2}\, {}_1\mathrm{F}_1(n+1;\, 1;\, -\eta^2) \tag{A.2.9a}$$

in order to apply a recursion formula for the hypergeometric function [16, §13.4.1] to obtain

$$(n+1)\, {}_1\mathrm{F}_1(n+2;\, 1;\, -\eta^2) = (2n + 1 - \eta^2)\, {}_1\mathrm{F}_1(n+1;\, 1;\, -\eta^2) - n\, {}_1\mathrm{F}_1(n;\, 1;\, -\eta^2) \tag{A.2.9b}$$

Applying this recursion to the autocorrelation function in (A.2.8), we obtain the recursion

$$\mathrm{R}_s(\tau;\, n+1) = (2n+1-\eta^2)\,\mathrm{R}_s(\tau;\, n) - n^2\,\mathrm{R}_s(\tau;\, n-1) \qquad \text{(A.2.10)}$$

REFERENCES

[1] R. A. Scholtz, "Multiple Access with Time-Hopping Impulse Modulation," *Proc. IEEE 1993 Milit. Comm. Conf.*, pp. 457-450.

[2] ——, "Propagation Measurement," web page of UltraLab at the University of Southern California. http://ultra.usc.edu/New_Site/propagations.html

[3] R. Fontana et al., "Recent Advances in Ultra Wideband Communications Systems," *Proc. 2002 IEEE Conf. on Ultra Wideband Systems and Technologies* (UWBST 2002), 21-23 May 2002, Baltimore.

[4] C. Corral, et al., "Pulse Spectrum Optimization for Ultra-Wideband Communication," *Proc. 2002 IEEE Conf. on Ultra Wideband Systems and Technologies* (UWBST 2002), 21-23 May 2002, Baltimore.

[5] J. D. Taylor, "Ultra-Wideband Radar Overview," in *Introduction to Ultra-Wideband Radar Systems*, CRC Press.

[6] M. Welborn, "Multiple Access Options for UWB WPANs," presentation to IEEE 802.15 high-rate WPAN alternate-PHY study group (SG3a), document 02/382.

[7] I. S. Gradshteyn and I. M. Ryzhik, *Table of Integrals, Series and Products*. New York: Academic Press, 1965.

[8] M. Pendergrass, "Time Domain Supporting Text for 802.15.3 Alternate Physical Layer Proposal," IEEE 802.15 high-rate WPAN alternate-PHY task group (TG3a), document 03/144r1.

[9] J. Foerster et al, "Intel CFP Presentation for a UWB PHY," proposal to IEEE 802.15 high-rate WPAN alternate-PHY task group (TG3a), document 03/109r1.

[10] G. Shor, "TG3a-Wisair-CFP-Presentation," proposal to IEEE 802.15 high-rate WPAN alternate-PHY task group (TG3a), document 03/151r1.

[11] R. Aiello, "Discrete Time PHY Proposal for TG3a," proposal to IEEE 802.15 high-rate WPAN alternate-PHY task group (TG3a), document 03/099r1.

[12] J. Cheah, "Channelized, Optimum Pulse Shaped UWB PHY Proposal," proposal to IEEE 802.15 high-rate WPAN alternate-PHY task group (TG3a), document 03/101.

[13] D. H. Kwon, "PHY Proposal for the IEEE 802.15.3a standard," proposal to IEEE 802.15 high-rate WPAN alternate-PHY task group (TG3a), document 03/135r1.

[14] L. B. Michael, M. Ghavami, and R. Kohno, "Multiple Pulse Generator for Ultra-Wideband Communication using Hermite Polynomial Based Orthogonal Pulses," *Proc. 2002 IEEE Conf. On Ultra Wideband Systems and Technologies* (UWBST 2002), 21-23 May 2002, Baltimore.

[15] U. W. Hochstrasser, "Orthogonal Polynomials," Chapter 22 of *Handbook of Mathematical Functions*, M. Abramowitz and I. A. Stegan, eds., National Bureau of Standards [now NIST] Applied Mathematics Series 55, Ninth printing, Government Printing Office, Washington, 1970.

[16] L. J. Slater, "Confluent Hypergeometric Functions," Chapter 13 of *Handbook of Mathematical Functions*, M. Abramowitz and I. A. Stegun, eds., National Bureau of Standards [now NIST] Applied Mathematics Series 55, Ninth printing, Government Printing Office, Washington, 1970.

[17] L. E. Miller, "Autocorrelation Functions for Hermite-Polynomial Ultrawideband Pulses," accepted for publication in *IEE Electronic Letters*, April 2003.